



# 1 A series of climate oscillations around 8.2 ka BP revealed through 2 multi-proxy speleothem records from North China

3 Pengzhen Duan<sup>1</sup>, Hanying Li<sup>2</sup>, Zhibang Ma<sup>3</sup>, Jingyao Zhao<sup>2</sup>, Xiyu Dong<sup>2</sup>, Ashish Sinha<sup>4</sup>, Peng  
4 Hu<sup>5,6</sup>, Haiwei Zhang<sup>2</sup>, Youfeng Ning<sup>2</sup>, Guangyou Zhu<sup>1</sup>, Hai Cheng<sup>2,7,8</sup>

5 <sup>1</sup>Research Institute of Petroleum Exploration and Development, PetroChina, Beijing, China

6 <sup>2</sup>Institute of Global Environmental Change, Xi'an Jiaotong University, Xi'an, China

7 <sup>3</sup>Key Laboratory of Cenozoic Geology and Environment, Institute of Geology and Geophysics, Chinese Academy of  
8 Sciences, Beijing, China

9 <sup>4</sup>Department of Earth Science, California State University, Dominguez Hills, Carson, USA

10 <sup>5</sup>Yunnan Key Laboratory of Meteorological Disasters and Climate Resources in the Greater Mekong Subregion,  
11 Yunnan University, Kunming 650091, China

12 <sup>6</sup>Department of Atmospheric Sciences, Yunnan University, Kunming 650500, China

13 <sup>7</sup>State Key Laboratory of Loess and Quaternary Geology, Institute of Earth Environment, Chinese Academy of  
14 Sciences, Xi'an, China

15 <sup>8</sup>Key Laboratory of Karst Dynamics, MLR, Institute of Karst Geology, CAGS, Guilin, China

16 *Correspondence to:* Hanying Li ([hanyingli@xjtu.edu.cn](mailto:hanyingli@xjtu.edu.cn)) and Hai Cheng ([cheng021@xjtu.edu.cn](mailto:cheng021@xjtu.edu.cn))

17 **Abstract.** The 8.2 ka event has been extensively investigated as a remarkable single event, but rarely considered as a  
18 part of multi-centennial climatic evolution. Here, we present absolutely dated speleothem multi-proxy records  
19 spanning 9.0–7.9 ka BP from Beijing in North China, near the northern limit of the East Asian summer monsoon  
20 (EASM) and thus sensitive to climate change, to provide evidence for the intensified multi-decadal climatic  
21 oscillations since 8.5 ka BP. Three extreme excursions characterized by inter-decadal consecutive  $\delta^{18}\text{O}$  excursions  
22 exceeding  $\pm 1\sigma$  are identified from 8.5 ka BP in our speleothem record. The former two are characterized by enriched  
23  $^{18}\text{O}$  at ~8.40 and 8.20 ka BP, respectively, suggesting a prolonged arid event which is supported by the positive trend  
24 in  $\delta^{13}\text{C}$  values, increased trace element ratios, and lower growth rate. Following the 8.2 ka event, an excessive rebound  
25 immediately emerges in our  $\delta^{18}\text{O}$  and trace element records but moderate in the  $\delta^{13}\text{C}$ , probably suggesting pluvial  
26 conditions and nonlinear response of the local ecosystem. Following two similar severe droughts at 8.40 and 8.20 ka  
27 BP, the different behavior of  $\delta^{13}\text{C}$  suggests the recovering degree of resilient ecosystem responding to different  
28 rebounded rainfall intensity. A comparison with other high-resolution records suggests that the two droughts-one  
29 pluvial patterns between 8.5 and 8.0 ka BP are of global significance instead of a regional phenomenon, which is  
30 causally linked to the slowdown and acceleration of the Atlantic Meridional Overturning Circulation that was further  
31 dominated by the freshwater injections in the North Atlantic.

32



## 33 1 Introduction

34 The overall warming during 9.0–7.9 ka BP (thousand years before present, where the present is 1950 CE) was  
35 punctuated by several inter-decadal to centennial climate fluctuations in the Northern Hemisphere (NH). The 8.2 ka  
36 event, as the most prominent abrupt cold event registered in the Greenland ice core records within the Holocene  
37 (Thomas et al., 2007), has been widely revealed by a large number of marine and terrestrial archives and dated to  
38 occur between 8.3–8.0 ka BP with a duration of 150–200 years (Figure S1) (e.g., Alley et al., 1997; Thomas et al.,  
39 2007; Kobashi et al., 2007; Cheng et al., 2009; Liu et al., 2013; Morrill et al., 2013; Duan P et al., 2021).

40 With deeper investigation, the “cold event” at 8.2 ka BP is evidenced likely to be a part of larger “set” of cold climate  
41 anomalies between 8.6 and 8.0 ka BP (e.g., Rohling and Pälike, 2005). According to marine records, the freshwater  
42 drainage(s) of proglacial Lakes Agassiz-Ojibway (LAO) into the North Atlantic, which has commonly been thought  
43 to trigger the 8.2 ka event (e.g., Alley et al., 1997; Barber et al., 1999) through weakening the Atlantic meridional  
44 overturning circulation (AMOC) and resultant global impact, is supposed to separate into two stages (Ellison et al.,  
45 2006; Roy et al., 2011; Godbout et al., 2019, 2020) or multiple outbursts (e.g., Teller et al., 2002; Kleiven et al., 2008;  
46 Jennings et al., 2015). The first pulse of freshwater may have induced the freshening of the North Atlantic at 8.55–  
47 8.45 ka BP (Lochte et al., 2019), the abrupt sea level jump (Tornqvist and Hijma, 2012; Lawrence et al., 2016), the  
48 detrital carbonate peak at ~8.6 ka (Jennings et al., 2015), and deposition of a red-sediment bed in Hudson Strait at  
49 ~8.26–8.69 ka BP (Kerwin, 1996; Lajeunesse and St-Onge, 2008). The superimposed effect of two or more successive  
50 freshwater drainages, or probably coupled with meltwater flux from the ice sheet (Morrill et al., 2014; Matero et al.,  
51 2017), finally led to severe and dramatic cooling events in the NH (Teller et al., 2002; Ellison et al., 2006). This is  
52 consistent with the view that the 8.2 ka event commenced at ~8.5 ka BP and persisted until ~8.0 ka BP (Rohling and  
53 Pälike, 2005) with more than one multi-decadal or centennial perturbations (e.g., Daley et al., 2009; Domínguez-Villar  
54 et al., 2009; Tan et al., 2020; Duan W et al., 2021). However, some terrestrial records, such as the Greenland ice cores  
55 (Thomas et al., 2007) and European lake sediments (von Grafenstein et al., 1999; Andersen et al., 2017), only  
56 documented a remarkable climate event at ~8.2 ka BP, whereas the counterpart to the preceding perturbation is not  
57 registered.

58 On the other hand, the multi-decadal or centennial perturbations aforementioned trended not only to the cold and dry  
59 direction in the NH, but also extremely warm and humid condition that has been evidenced in the immediate aftermath  
60 of the 8.2 ka event (Andersen et al., 2017; Duan P et al., 2023). In particular, the post-event excessive rebound suggests  
61 a major pluvial episode prevailing across a large part of North China (Duan P et al., 2023). However, only one proxy,  
62 speleothem  $\delta^{18}\text{O}$  (Duan P et al., 2023), is insufficient and thus multi-proxy evidences about the overshoot is necessary,  
63 especially from the Asian summer monsoon (ASM) domain where the climate change has a fast atmospheric  
64 teleconnection with the high-latitude North Atlantic (Cheng et al., 2020; 2022), to complement our understanding on  
65 the dynamics of rapid climatic changes, their underlying mechanisms, and the local ecosystem response.

66 In the context of high-emission greenhouse gas nowadays, the melted Greenland ice sheet will inject huge amount of  
67 freshwater into the North Atlantic in the next millennium, which is analogous to the sea level rising scenario during  
68 9.0–7.9 ka BP (e.g., Aguiar et al., 2020). Therefore, it is important to elucidate the climate variations in response to  
69 the freshwater injections in the past to provide a potential analogy for future behavior, especially in North China where



70 the ecosystem and economic development are highly dependent on hydroclimatic changes. Importantly, our study area  
71 is located near the northern fringe of the East Asian summer monsoon (EASM), thus sensitively responding to the  
72 variations of EASM intensity (Duan et al., 2014; Li et al., 2017; Ma et al., 2012). Here we provide high temporal  
73 resolution speleothem multi-proxy records, including  $\delta^{18}\text{O}$ ,  $\delta^{13}\text{C}$ , Mg/Ca, Sr/Ca, and Ba/Ca, from Beijing in North  
74 China to reconstruct the hydroclimatic variations over the Circum-Bohai Sea Region (CBSR) between 9.0–7.9 ka BP.  
75 Two cold climate anomalous events pre- and at 8.2 ka BP, as well as post-8.2 ka rebound, are investigated to show  
76 the general climate pattern around the abrupt cold event from its triggering, response, and ensuing feedback and further  
77 examine the relationship between the ASM and the North Atlantic.

## 78 **2 Materials and Methods**

### 79 **2.1 Regional settings and modern climatology**

80 Situated at ~60 km southwest of Beijing in North China, the Huangyuan Cave (39°42' N, 115°54' E, altitude 610 m  
81 above sea level) is developed in a Middle Proterozoic dolomite and adjacent to Kulishu (39°41' N, 115°39' E) and  
82 Shihua (39°47' N, 115°56' E) Caves (Figure S1). The vegetation above the cave is dominated by secondary-growth  
83 deciduous broadleaf trees and shrubs (Ma et al., 2012; Duan et al., 2014). According to the meteorological station's  
84 observed data between 1998 and 2010, the average annual air temperature and precipitation in the study area are  
85 12.2 °C and 540 mm, respectively, with cold dry winters and warm wet summers (Figure 1). The regional precipitation  
86 is highly seasonal and mainly concentrates on the summer season. It has been demonstrated (Duan et al., 2016; Li et  
87 al., 2017; Duan P et al., 2023) that the summer precipitation  $\delta^{18}\text{O}$  ( $\delta^{18}\text{O}_p$ ) is negatively correlated with the summer  
88 rainfall amount over the study area and positively correlated with  $\delta^{18}\text{O}_p$  over almost the entire EASM domain, the  
89 latter of which is normally termed the EASM intensity.

90 Speleothem BH-2, collected from Huangyuan Cave, is ~17 cm in length and ~5 cm in width (Figure 2a). The  
91 candlestick shape of speleothem without macroscopic bias of the growth axis signifies that it was deposited under  
92 relatively stable conditions (Baker et al., 2007). The results for the section of 15–48 mm from the top of the sample,  
93 corresponding to 8.38–8.06 ka BP, have been reported in previous investigation (Duan P et al., 2023). In this study,  
94 the multi-proxy results of the entire sample are presented that spans 9.0–7.9 ka BP.

### 95 **2.2 $^{230}\text{Th}$ dating, stable isotope, and trace element analysis**

96 A total of 22  $^{230}\text{Th}$  dates (Table S1) were performed at University of Minnesota, USA, using Thermo-Finnigan  
97 Neptune multi-collector inductively coupled plasma mass spectrometers (MC-ICP-MS, Thermo Scientific). The  
98 methods are described in detail in Cheng et al. (2013). We followed standard chemistry procedures to separate uranium  
99 and thorium for instrument analysis (Edwards et al., 1987). A triple-spike ( $^{229}\text{Th}$ - $^{233}\text{U}$ - $^{236}\text{U}$ ) isotope dilution method  
100 was employed to correct instrumental fractionation and determine U/Th isotopic ratios and concentrations.  
101 Uncertainties in U/Th isotopic data were calculated offline at  $2\sigma$  level. Confocal Laser Fluorescent Microscopy was  
102 used to observe clear annual bands for the section of 15 to 48 mm, each of which comprises paired light and dark  
103 lamina, and the results have been reported in previous study (Duan P et al., 2023).



104 The stable oxygen and carbon isotopes ( $\delta^{18}\text{O}$  and  $\delta^{13}\text{C}$ ) of speleothem BH-2 were determined on a Thermo-Scientific  
105 MAT-253 isotope ratio mass spectrometer equipped with an online carbonate device (Kiel IV) at the Institute of  
106 Geology and Geophysics, Chinese Academy of Sciences and Isotope Laboratory of Xi'an Jiaotong University. The  
107 powdered subsamples weighing  $\sim 30\ \mu\text{g}$  were drilled along the central growth axis using a Micromill device and then  
108 reacted with  $\sim 103\%$  phosphoric acid at  $70\ ^\circ\text{C}$ . The stable oxygen and carbon isotopic compositions of the generated  
109  $\text{CO}_2$  gas were measured with working  $\text{CO}_2$  standard gas whose values have been calibrated by international standards.  
110 All results are reported as the per mil deviation relative to the Vienna Pee Dee Belemnite (VPDB). The reported  
111 precision of both  $\delta^{18}\text{O}$  and  $\delta^{13}\text{C}$  at  $1\sigma$  level is better than  $0.1\ \text{‰}$ .  
112 Trace element ratios (Mg/Ca, Sr/Ca, Ba/Ca), of which the intensity of emission lines are 285.2 nm, 407.8 nm, and  
113 373.7 nm, were measured using Laser Induced Breakdown Spectroscopy (LIBS) following the detailed description in  
114 Li et al. (2018). In brief, analyses were performed by pulsing laser and then analyzing the intensity of specific spectrum  
115 of trace elements to obtain their content and ratios relative to the calcium for each point. The obtained record is the  
116 median intensity ratio based on 20 pulses at each sampling site after 5 laser shots for pre-cleaning the surface. The  
117 measurements were performed continuously along the speleothem's growth axis at 0.3 mm increment and a total of  
118 565 data were obtained.

### 119 3 Results

#### 120 3.1 $^{230}\text{Th}$ dates and age model

121 The  $^{230}\text{Th}$  dating results of the BH-2 are presented in Table S1 which shows that the BH-2 covers the interval between  
122 9.0 and 7.9 ka BP. All dates are in stratigraphic order within uncertainties. The average dating uncertainty is  $\pm 57$   
123 years at  $2\sigma$  level. For the period from 8.25 to 8.11 ka BP, we present the speleothem record from Duan P et al. (2023),  
124 which is based on the combination of the annual lamina counting and  $^{230}\text{Th}$  dates. In addition, here we use an updated  
125 chronology of the BH-2 based on the Oxcal algorithm (Ramsey, 2008), which includes ten additional ages from the  
126 remnant sections (Figure 2b).

#### 127 3.2 Stable isotopic compositions and growth rate

128 The BH-2 record contains 663 pairs of  $\delta^{18}\text{O}$  and  $\delta^{13}\text{C}$  data with a mean temporal resolution of  $\sim 1.6$  years. The  $\delta^{18}\text{O}$   
129 values range from  $-7.1\ \text{‰}$  to  $-11.5\ \text{‰}$  with a mean of  $-9.3\ \text{‰}$  and  $\delta^{13}\text{C}$  values vary from  $-8.0\ \text{‰}$  to  $-12.1\ \text{‰}$  with an  
130 average value of  $-10.2\ \text{‰}$  (Figures 2d and 2e). It can be seen that the  $\delta^{13}\text{C}$  profile follows the same general patterns as  
131 the  $\delta^{18}\text{O}$  ( $r = 0.63$ ,  $p < 0.01$ ). Compared to the later stage, although some fluctuations are included, the  $\delta^{13}\text{C}$  and  $\delta^{18}\text{O}$   
132 profiles are relatively invariable before 8.5 ka BP. In contrast, the  $\delta^{18}\text{O}$  record exhibits a remarkable positive shift at  
133  $\sim 8.45\text{--}8.39$  ka BP, during which period the  $\delta^{13}\text{C}$  record shifts less prominently to the positive direction but with a  
134 fluctuating increasing trend. The rebound from the positive shift of  $\delta^{13}\text{C}$  and  $\delta^{18}\text{O}$  profiles is followed by a less variable  
135 episode spanning 8.39–8.26 ka BP. Afterward, as the most remarkable feature, both records show extremely positive  
136 excursions spanning  $\sim 8.26\text{--}8.14$  ka BP (Figure 2). The positive anomaly is followed by a shift to the opposite extreme



137 to reach the most negative stage in the  $\delta^{18}\text{O}$  record during 8.14–8.05 ka BP, which is not conspicuous in the  $\delta^{13}\text{C}$   
138 record.

139 The growth rate of the BH-2 was established based on the reconstructed chronology (Figure 2c). It is apparent that  
140 speleothem BH-2 was contiguously deposited without visible growth hiatus and the growth rate during 8.46–8.16 ka  
141 BP ( $< 0.15$  mm/year) is apparently lower relative to other intervals ( $> 0.15$  mm/year on average). Specifically, there  
142 are obvious transitions from higher to lower growth rates at  $\sim 8.46$  ka BP and in the opposite trend at  $\sim 8.16$  ka BP.  
143 Moreover, it is notable that the lowest growth rate from  $\sim 8.28$  to 8.18 ka BP broadly corresponds to the relatively high  
144  $\delta^{18}\text{O}$  and  $\delta^{13}\text{C}$  excursions.

### 145 3.3 Trace element ratios

146 The signals in the trace element ratio records are quite variable (Figure S2). Similar to  $\delta^{18}\text{O}$  and  $\delta^{13}\text{C}$  records, all of  
147 the Mg/Ca, Sr/Ca, and Ba/Ca records display positive excursions at  $\sim 8.40$  and 8.20 ka BP despite the relative  
148 ambiguity of the former one in the Sr/Ca and the latter one in the Mg/Ca, respectively. Besides, there is another more  
149 positive excursion at  $\sim 8.86$  in the Mg/Ca ratio record, which is absent in the other two records. After principal  
150 component analysis of the three records, the excursions at  $\sim 8.40$  and 8.20 ka BP are especially conspicuous (Figure  
151 2f). Before 8.46 ka BP, the PC1 result fluctuates frequently with considerable magnitude, which seems coincident  
152 with the  $\delta^{18}\text{O}$  variability. In the duration of 8.46–8.38 ka BP, it exhibits a fluctuating positive trend and a rapid rebound  
153 at  $\sim 8.38$  ka BP. Aftermath, the values remain relatively stable until  $\sim 8.23$  ka BP when another positive excursion  
154 commences. In this excursion, the PC1 values culminate at  $\sim 8.12$  ka BP followed by a rapid rebound which indicates  
155 the termination of this excursion. The values remain relatively stable after 8.10 ka BP.

## 156 4 Discussion

### 157 4.1 Proxy interpretations

158 The replication test of  $\delta^{18}\text{O}$  records between the BH-2 from Huangyuan Cave and the KLS12 from nearby Kulishu  
159 Cave (Duan W et al., 2021) by using the ISCAM (Intra-site Correlation Age Modeling) algorithm (Fohlmeister, 2012)  
160 show significantly positive correlation ( $r = 0.62$ ,  $p < 0.05$ ) during 9.0–7.9 ka BP (Figure S3), strongly suggesting that  
161 the influence of kinetic fractionation is likely insignificant and the carbonate deposition process is close to equilibrium  
162 (Dorale and Liu, 2009). Hence, the BH-2  $\delta^{18}\text{O}$  signals reflect the changes in drip water  $\delta^{18}\text{O}$  which in turn inherit from  
163  $\delta^{18}\text{O}_p$  related to the regional hydroclimate variations in general. Notably, the study site is located along the summer  
164 monsoon fringe with relatively low annual precipitation, and thus the thermodynamics variations in EASM in the  
165 areas can significantly bias the mean annual  $\delta^{18}\text{O}$  value, e.g., the summer rainfall amount. Indeed, the modern  
166 observations (Duan al., 2016) and reanalysis results (He et al., 2021; Duan P et al., 2023; Zhao et al., 2023) have  
167 proved that speleothem  $\delta^{18}\text{O}$  in the study area can be used as a reliable proxy to indicate the regional precipitation  
168 variations and the dynamic changes of the summer monsoon circulation, that is, depleted  $^{18}\text{O}$  corresponds to increased  
169 rainfall over the study area and strengthened EASM, and vice versa.



170 Under the equilibrium fractionation conditions, the carbon isotope ratios ( $\delta^{13}\text{C}$ ) of speleothem carbonate reflect a  
171 mixture of three carbon sources: plant root-respired  $\text{CO}_2$  in the soil zone, atmospheric  $\text{CO}_2$ , and dissolution of bedrock  
172 carbonate (McDermott, 2004), in which the plant-related  $\text{CO}_2$  is the most important for the variability of the  
173 speleothem  $\delta^{13}\text{C}$  (Fairchild et al., 2006; Li Y et al., 2020). It has been suggested that changes in the density of  
174 vegetative cover and biomass exert a critical impact on the speleothem  $\delta^{13}\text{C}$  variations in the study region, instead of  
175 the relative ratio of C3 (woody taxa) and C4 (grasses) plants (Duan et al., 2014). This is consistent with our observation  
176 that the  $\delta^{13}\text{C}$  values of speleothem BH-2 fall between -8 and -12 ‰, which is within the typical range for the C3-  
177 dominant plant coverage (McDermott, 2004; Fairchild et al., 2006). Although climate-induced changes in the karst  
178 system, like  $\text{pCO}_2$  degassing, water infiltration, and prior calcite precipitation (PCP) could also contribute to the  $\delta^{13}\text{C}$   
179 changes (Fairchild and Treble, 2009; Li et al., 2020), the significant covariance of  $\delta^{13}\text{C}$  and  $\delta^{18}\text{O}$  in the BH-2 and  
180 minor effect of kinetic fractionations as aforementioned, as well as the unbiased  $\delta^{18}\text{O}$  signal inherited from  
181 precipitation strongly suggest that the density of vegetative cover, the biomass activity, and the vadose of seepage  
182 solution dominated by regional hydroclimatic conditions could play a crucial role in the decadal to centennial scale  
183 variations of  $\delta^{13}\text{C}$  in speleothem BH-2.

184 The influence of PCP can be inferred from trace element concentrations such that strong (weak) PCP normally induces  
185 a high (low) trace element content relative to the calcium in the speleothem calcite (Johnson et al., 2006; Fairchild  
186 and Treble, 2009). In general, higher trace element ratio values indicate overall drier conditions when reduced  
187 infiltration and increased residence time in the epikarst above the cave favors faster  $\text{CO}_2$  degassing and PCP, inducing  
188 relatively higher trace element content in the cave drip-water due to the preferential loss of  $\text{Ca}^{2+}$  along the deposition  
189 path; the opposite processes occur in wetter conditions (e.g., Cruz et al., 2007; Griffiths et al., 2010; Zhang et al.,  
190 2018). On the other hand, water-rock interaction may have been enhanced in the aquifer during direr conditions  
191 because of the prolonged residence time of fluid in the path way, which tends to favor the leaching of Mg and Sr  
192 element from the dolomite host rock (Fairchild et al., 2000) and eventually leads the two elements to enrichment in  
193 dripwater, and hence speleothem. Apparently, both above two mechanisms indicate the trace element ratios can be  
194 used as a reliable proxy of local wetness conditions. Regarding the speleothem growth rate, the sharp drops and  
195 persistent lower values in this proxy corresponding to major positive  $\delta^{18}\text{O}$  and  $\delta^{13}\text{C}$  excursions signify that it most  
196 likely was controlled by a sufficient or insufficient supply of drip water, and hence the local rainfall amount (e.g.,  
197 Polyak et al., 2004; Banner et al., 2007).

198 In summary, the broad similarity of multi-proxies ( $\delta^{18}\text{O}$ ,  $\delta^{13}\text{C}$ , trace element ratios, and growth rate) in speleothem  
199 BH-2 lends robust support to that all of them record changes in hydroclimatic characteristics (Fairchild and Treble,  
200 2009), that is, the intensity of the EASM and associated rainfall amount presumably dominating the hydroclimatic  
201 variabilities over and in the cave in the study area. On the other hand, the discrepancy between various proxies could  
202 suggest that different factors exert influence on these signals in the meteoric water-cave aquifer-drip water-carbonate  
203 precipitation processes.



#### 204 4.2 Climate fluctuations between 9.0 and 7.9 ka BP in Beijing

205 The variability of the BH-2  $\delta^{18}\text{O}$  record reveals inter-decadal to multi-decadal dry ( $> +1\sigma$ ) or pluvial ( $< -1\sigma$ )  
206 oscillations from 9.0 to 7.9 ka BP without a distinct long-term trend (Figure 2). One noticeable feature of our  $\delta^{18}\text{O}$   
207 record is a switch from relatively muted to highly variable episodes divided at  $\sim 8.5$  ka BP, consistent with the absence  
208 and dominance of centennial to inter-decadal periodicity before and after 8.5 ka BP, respectively (Figure 2).

209 The first persistent drought, indicated by positive  $\delta^{18}\text{O}$  excursion exceeding  $+1\sigma$  values for more than 15 years, initially  
210 started at 8.46 ka BP and terminated at 8.39 ka BP (8.4 ka event herein). The entire event is characterized by a saw-  
211 tooth structure with a dramatic 2.5 ‰ increase within  $\sim 55$  years and a 2.2 ‰ rebound within 11 years, indicating a  
212 fast weakened EASM and thus reduced precipitation in the study area. This arid condition is supported by the  
213 contemporaneous trace element records which show a remarkable positive shift that seems strictly resemble the  $\delta^{18}\text{O}$   
214 record regarding both the shape and duration, pointing to the changed dynamic process in the cave in response to the  
215 decreased precipitation water supply. Additionally, the high-to-low transition of growth rate commencing  $\sim 8.46$  ka  
216 BP presumably results from less drip water supply and further in turn reduced precipitation over the cave, marking  
217 the start of the EASM weakening. However, the change of vegetation indicated by the  $\delta^{13}\text{C}$  proxy is not immediate.  
218 It seems that the increasing  $\delta^{13}\text{C}$  trend begins later than other proxies and only exhibits a short excursion, probably  
219 indicating the nonlinear response of vegetation evolution to the hydroclimate change, especially in a short-time climate  
220 event. This could be related to the delayed shortage of subground water for plant growth and a muted response of  
221 ecological processes to the hydroclimatic variability in a relatively wet context as indicated by low  $\delta^{18}\text{O}$  and trace  
222 element values surrounding this excursion (Duan P et al., 2021).

223 Following the end of above arid excursion, another centennial oscillation in much temperate mode persisted to  $\sim 8.25$   
224 ka BP. Subsequently, the BH-2  $\delta^{18}\text{O}$  exhibited the most remarkable droughts with centennial positive excursion  
225 between  $\sim 8.26$  and 8.11 ka BP, conservatively corresponding to the 8.2 ka event (Duan P et al., 2023). This drought  
226 event is also proved in the trace element records via the increased values, in concert with the decreased seepage water  
227 and hence enhanced PCP. In detailed structure, these trace element ratio records commonly show prominent positive  
228 excursion at  $\sim 8.20$  and 8.14 ka BP, the latter of which is especially elevated in them. However, the slowly increased  
229 pattern in the trace element ratio records from 8.26 to 8.18 ka BP is quite distinct from the  $\delta^{18}\text{O}$  record in which its  
230 values dramatically increase in the first 70 years, suggesting the probably nonlinear relationship between regional  
231 climate ( $\delta^{18}\text{O}$ ) and local hydroclimatic condition (trace element ratios). Moreover, in this event, the  $\delta^{13}\text{C}$  exhibits a  
232 prominent positive shift, pointing to the decay of the ecosystem in this severe drought event. It is noteworthy that the  
233 variation pattern of  $\delta^{13}\text{C}$  in the 8.2 ka event is more similar to the  $\delta^{18}\text{O}$  relative to the 8.4 ka event. This absence of  
234 muted  $\delta^{13}\text{C}$  signal suggests the close relationship between the vegetation and regional hydroclimatic conditions in a  
235 long duration and more severe climatic deterioration. Intriguingly, the lower excursion of growth rate somehow  
236 predates other proxies. This inter-proxy discrepancy suggests that there are other potential factors, such as the  
237 temperature (Wong et al., 2015), controlling the cave dynamic processes, and the growth rate could be a more  
238 qualitative indicator to broadly constrain the hydroclimatic conditions in combination with other proxies.

239 Afterward, the hydroclimatic conditions go to the reverse side of the extreme, manifesting a multi-decadal excessive  
240 rebound (i.e., overshoot) attaining the lowest  $\delta^{18}\text{O}$  values ( $-11.5$  ‰) of the entire record, suggesting the strongest



241 pluvial event (Duan P et al., 2023). This overshoot is additionally supported by trace element ratio record which show  
242 quite low values relative to the period before 8.46 ka BP. However, the rebound of the  $\delta^{13}\text{C}$  during the post-8.2 ka  
243 event is not as conspicuous as the  $\delta^{18}\text{O}$  overshoot and only reaches the mean level of that preceding the 8.4 ka event.  
244 These features further illustrate the aforementioned nonlinear relationship among the variabilities of regional climate,  
245 local hydrological condition, and ecosystem. In other words, the coverage of vegetation and soil microbiological  
246 activity during the overshoot event didn't recover to the initial conditions before the 8.2 ka event.  
247 The different behavior of  $\delta^{13}\text{C}$  after two similar severe droughts at 8.40 and 8.20 ka BP suggests the degree of resilient  
248 ecosystem to the different rebound rainfall intensity. For the 8.40 ka event, the subsequent rebound of  $\delta^{13}\text{C}$  to its prior  
249 value suggests the high-level resilience of the plant community to environmental variations under the moderate  
250 precipitation amount as indicated by the  $\delta^{18}\text{O}$  and trace element ratio records. In contrast, the suddenly excessive  
251 increase of precipitation after the 8.2 ka event, which was much more than that before the event, could have suppressed  
252 the recovery of vegetation and soil biological activity and thus the moderate rebound of  $\delta^{13}\text{C}$  values. Theoretically,  
253 the longer weakened atmospheric circulation during the 8.2 ka event and reduced precipitation presumably induced  
254 deteriorated vegetation as well as poor-developed soil. However, it seems that the precipitation intensity after the 8.2  
255 ka event exerted a key role on the recovery of vegetation density and soil productivity. Specifically, the severe 8.2 ka  
256 drought event had a profoundly negative impact on the vegetation-soil system and led them to become more vulnerable  
257 under the water shortage conditions. On the other hand, the excessive precipitation after this drought could cause soil  
258 erosion and further ecological damage, suppressing the ecosystem recovery above the cave as well as the  $\delta^{13}\text{C}$  signals  
259 in speleothem. Conclusively, the ecosystem in this karst region was quite vulnerable and the variability of the  
260 vegetation-soil system here was tied to local hydrologic conditions with both high and low thresholds.  
261 To summarize, akin to the  $\delta^{18}\text{O}$  record, other proxy records of the BH-2 (Figure 2) delineate two major drought events,  
262 indicated by prominent excursions centered at 8.40 and 8.20 ka BP, respectively, suggesting vegetation degeneration  
263 (Duan et al., 2014) and elevated prior calcite precipitation (PCP) arising from longer residence time of solution in the  
264 karst aquifer (e.g., Johnson et al., 2006; Fairchild et al., 2009), both of which responded to the deteriorated  
265 hydroclimatic conditions. The discrepancy between them could suggest that other drivers than only hydroclimatic  
266 conditions possibly have played a non-negligible role in the processes of speleothem formation. In particular, the  
267 intensity of the EASM ( $\delta^{18}\text{O}$ ) and the precipitation amount (trace element ratio) over the study area presumably were  
268 definitely correlated on a broad pattern but did not necessarily exactly follow each other.

#### 269 **4.3 Spatial patterns for the two drought-one pluvial pattern and underlying mechanisms**

270 This two drought-one pluvial pattern from 8.5 to 8.0 ka BP in speleothem BH-2 represents global scale climate  
271 disturbance signals rather than a regional phenomenon since these climate excursions have been widely documented  
272 (Figures 3 and 4). In the ASM domain, speleothem records from such as Lianhua (Dong et al., 2018), Wuya (Tan et  
273 al., 2020) Caves in North and Northwest China, and Qingtian Cave (Liu et al., 2015) in central China exhibit consistent  
274 structure with the BH-2 at around 8.2 ka BP. In particular, a broad anomaly spanning ~340 years between 8.46 and  
275 8.12 ka BP has been revealed (Tan et al., 2020) and we find the post-8.2 ka overshoot is also distinguishable (Figure  
276 4) in the speleothem  $\delta^{18}\text{O}$  record from the western Chinese Loess Plateau which is situated in the northern limit of the





277 ASM. Unlike these north-located records, although a prominent 8.2 ka event is documented in speleothem of Heshang  
278 Cave in central China (Liu et al., 2013), the preceded excursion is ambiguous and the post-8.2 ka event anomaly is  
279 absent. Coincidentally, a similar phenomenon seems to occur in Dongge Cave in South China (Cheng et al., 2009). This  
280 probably suggests that relative to the low latitudes, the climate in the north part of the ASM is more sensitive to the  
281 climate perturbation signals originating from the high northern latitude regions because high northern latitude climate  
282 variations can strongly affect the westerly changes and finally influence the EASM (Chiang et al., 2015; Duan et al.,  
283 2016; Tan et al., 2020). In the low latitudes of the Indian summer monsoon realm, the speleothem  $\delta^{18}\text{O}$  record from  
284 Hoti Cave is remarkably consistent with the pattern in our record. Specifically, Hoti Cave record shows positive  $\delta^{18}\text{O}$   
285 excursions by  $\sim 2\text{‰}$  in amplitude centering  $\sim 8.4$  ka BP and a growth hiatus at 8.2 ka BP surrounded by enriched  $^{18}\text{O}$ ,  
286 pointing to the drought conditions due to the weakened Indian summer monsoon attendant with a southward shift of  
287 the intertropical convergence zone (ITCZ). After the growth resumption, an overshoot can be identified (Cheng et al.,  
288 2009). It happens that the two positive excursions are quite pronounced in nearby Qunf Cave (Figure 3) (Cheng et al.,  
289 2009), whereas the overshoot is absent. Collectively, records from more sensitive areas in the ASM domain intactly  
290 preserved the two drought-one pluvial pattern, while the pre-8.2 ka event or the overshoot is missed in records from  
291 insensitive regions.

292 In the North Atlantic region, Greenland ice core  $\delta^{18}\text{O}$  (Thomas et al., 2007) and reconstructed temperature based on  
293 argon and nitrogen isotopes (Kobashi et al., 2017) captured both the 8.2 ka event and ensuing overshoot, and the pre-  
294 8.2 ka event is apparent in the temperature profile but ambiguous or slightly excused (Jennings et al., 2015) in the  
295  $\delta^{18}\text{O}$  records. Indeed, the atmospheric circulation over Greenland has substantially changed since  $\sim 8.5$  ka BP as  
296 suggested by increased potassium and calcium ions, indicators of dust supply to Greenland, as well as decreased snow-  
297 accumulation rate (Rohling and Pälike, 2005; Kobashi et al., 2017; Burstyn et al., 2019). The absent signal of the pre-  
298 8.2 ka event in  $\delta^{18}\text{O}$  records could be attributed to the compensation of other processes like precipitation seasonality  
299 and summer warming (He et al., 2021). The prolonged climate anomalies around 8.2 ka BP are further supported by  
300 two negative anomalies at 8.3 and 8.2 ka BP, respectively, in northern Spain speleothem  $\delta^{18}\text{O}$  record (Domínguez-  
301 Villar et al., 2009), lower tree ring width from 8.42 to 8.0 ka BP in Germany (Spurk et al., 2002), as well as degraded  
302 climate conditions between 8.45 and 8.10 ka BP revealed by speleothem proxies from Père Noël Cave in Belgium  
303 (Allan et al., 2017). All of these collectively suggest a series of pronounced climate oscillations between 8.5 and 8.0  
304 ka BP, instead of merely the 8.2 ka event, is of hemispheric significance (Rohling and Pälike, 2005).

305 Similar but antiphase patterns are observed in the records from the Southern Hemisphere. For example, it appears that  
306 speleothem record from Lapa Grand Cave in East Brazil (Stríkis et al., 2011) captured the two pluvial-one drought  
307 structure (Figures 3 and 4). Intriguingly, speleothem record from Padre Cave (Cheng et al., 2009) fails to preserve as  
308 clear pre- and post- 8.2 ka events as its adjacent Lapa Grand Cave (Figure 4), presumably due to different cave settings.  
309 But, the beginning deposit of speleothem in Padre Cave at  $\sim 8.5$  ka BP, coeval with the reduced precipitation in the  
310 ASM domain, likely reflects more favorable hydroclimatic conditions due to more precipitation, which in turn could  
311 arise from intensified South American summer monsoon associated with the southward displacement of the ITCZ  
312 (Wang X et al., 2004), suggesting the possible occurrence of the pre-8.2 ka event there. Coincidentally, the speleothem  
313 growth resumption after a long hiatus (Duan P et al., 2021), together with the negative trend of speleothem  $\delta^{18}\text{O}$  record



314 (Voarintsoa et al., 2019) in Northwest Madagascar commenced at ~8.5 ka BP and persisted until the end of the 8.2 ka  
315 event, indicative of more precipitation in response to the southward ITCZ shift, suggesting the extent of the pre-8.2  
316 ka event to the East Africa monsoon domain. However, the post-8.2 ka event was not clearly identified by the  
317 Northwest Madagascar record and thus more evidence is needed.

318 The two droughts-one pluvial pattern revealed in our BH-2 records could mainly correspond to the waxing and waning  
319 of drainages of the LAO (Barber et al., 1999; Ellison et al., 2006) and contemporary ice sheet melted freshwater flux  
320 (Matero et al., 2017, 2020) (Figure 3), both of which causally related to the AMOC strength dynamics. Firstly, the  
321 major two-step outburst of the LAO (e.g., Ellison et al., 2006; Kleiven et al., 2008; Jennings et al., 2015; Lochte et al.,  
322 2018; Godbout et al., 2019, 2020) and the continuous Laurentide Ice Sheet (LIS) melting together contributed to the  
323 increase of total freshwater flux (e.g., Morrill et al., 2014; Matero et al., 2017, 2020), inducing observed sea level rise  
324 in North Atlantic commencing ~8.5 ka BP (Hijma et al., 2010), cooling conditions initially in the circum-North  
325 Atlantic region and perturbed into other areas through fast atmospheric propagations (Cheng et al., 2009, 2020; Liu et  
326 al., 2013; Buizert et al., 2014; Duan P et al., 2021). Coincident with enriched  $^{18}\text{O}_p$  in most ASM domains, the intensity  
327 of the East Asian summer monsoon was weakened (Cheng et al., 2009) and less precipitation fell in the Beijing area  
328 (Duan P et al., 2023). In contrast, due to the southward displacement of the ITCZ in response to the hemispheric  
329 thermal contrast, the Southern Hemisphere, like Northeast Madagascar and East Brazil, received more precipitation  
330 (i.e., stronger monsoon) and thus speleothem records there exhibit depleted  $^{18}\text{O}_p$ . Further, the simulated smaller  
331 freshwater flux peak at ~8.5 ka BP relative to the second one at 8.2 ka (Figure 3) (Matero et al., 2020) could provide  
332 a potential explanation for the lower amplitude and shorter duration of the pre-8.2 ka event relative to the 8.2 ka event  
333 in our record and the absence of the pre-8.2 ka event in other records. Additionally, the 8.2 ka event is preceded by a  
334 remarkable reduction in solar activity by  $\sim 1 \text{ Wm}^{-2}$  with a duration of  $\sim 150$  years, beginning at  $\sim 8.45$  ka BP (Rohling  
335 and Pälike, 2005; Steinhilber et al., 2009; Wanner et al., 2011; Burstyn et al., 2019), and an increase in the magnitude  
336 and frequency of volcanic eruptions (Kobashi et al., 2017; Burstyn et al., 2019), both of which are also thought to  
337 contribute to the prolonged climate disturbance via different impacts on atmospheric processes.

338 On the other hand, the overshoot in the ASM domain could be remotely related to the higher temperature in the North  
339 Atlantic (Kobashi et al., 2017; Andersen et al., 2017) (Figure 4) which in turn possibly arose from the remarkably  
340 speed-up AMOC (Ellison et al., 2006; Renold et al., 2010; Mjell et al., 2015; Andersen et al., 2017). The accelerated  
341 AMOC led to more heat release in the North Atlantic and anomalously strengthened ASM. In the meanwhile, the  
342 ITCZ and associated rainbelt were displaced northwards, causing less precipitation in east Brazil as evidenced by  
343 positive  $\delta^{18}\text{O}$  excursion of speleothem from Lapa Grande Cave (Figure 4).

## 344 5 Conclusions

345 The multi-proxy records of speleothem BH-2 document the multi-decadal to centennial scale hydroclimate changes  
346 in Beijing of North China with two arid episodes at  $\sim 8.4$  and 8.2 ka BP, and an immediately ensuing excessive rebound  
347 after the 8.2 ka event. A comparison with other paleoclimate records suggests that these prominent climate fluctuations  
348 with two drought-one pluvial pattern should be a global signal instead of a regional phenomenon. We propose that the  
349 slowdown and resumption of the AMOC controlled by the freshwater flux into the North Atlantic and the resultant



350 reorganization of the atmospheric circulation during the study stage mainly contribute to the arid and pluvial  
351 excursions, and the influence of volcanic outbursts and reduced solar activity are also non-negligible.

#### 352 **Data availability**

353 All data needed to evaluate the conclusions in the paper are presented in the paper. The data will be archived at the  
354 NOAA National Climate Data Center (<https://www.ncdc.noaa.gov/data-access/paleoclimatology-data>) when this  
355 manuscript is accepted.

#### 356 **Author contributions**

357 PD, HL and HC designed the research and experiments. PD wrote the first draft of the paper. HL, HC, and AS  
358 revised the paper. ZM did the fieldwork and collected the samples. ZM and HC conducted the <sup>230</sup>Th dating. ZM,  
359 HC, and PD conducted the oxygen isotope measurements. All authors discussed the results and provided inputs on  
360 the paper.

#### 361 **Competing interests**

362 The authors declare that they have no conflict of interest.

#### 363 **Acknowledgments**

364 This work was supported by the National Natural Science Foundation of China grants (42150710534 and 41888101  
365 to H.C.). We specially thank Ming Tan and Wuhui Duan from Institute of Geology and Geophysics, Chinese Academy  
366 of Sciences for their helpful suggestions.

#### 367 **References**

- 368 Aguiar, W., Meissner, K. J., Montenegro, A., Prado, L., Wainer, I., and Carlson, A. E.: Magnitude of the 8.2 ka event  
369 freshwater forcing based on stable isotope modelling and comparison to future Greenland melting, *Sci. Rep.*, 11, 1–  
370 10, <https://doi.org/10.1038/s41598-021-84709-5>, 2021.
- 371 Allan, M., Fagel, N., van der Lubbe, H. J. L., Vonhof, H. B., Cheng, H., Edwards, R. L., and Verheyden, S.: High-  
372 resolution reconstruction of 8.2-ka BP event documented in Père Noël cave, southern Belgium, *J. Quat. Sci.*, 33, 840–  
373 852, <https://doi.org/10.1002/jqs.3064>, 2018.
- 374 Alley, R. B., Mayewski, P. A., Sowers, T., Stuiver, M., Taylor, K. C., and Clark, P. U.: Holocene climatic instability:  
375 a prominent, widespread event 8200 yr ago, *Geology*, 25, 483–486, [https://doi.org/10.1130/0091-7613\(1997\)025<0483: HCIAPW>2.3.CO;2](https://doi.org/10.1130/0091-7613(1997)025<0483:HCIAPW>2.3.CO;2), 1997.



- 377 Andersen, N., Lauterbach, S., Erlenkeuser, H., Danielopol, D. L., Namiotko, T., and Hüls, M.: Evidence for higher-  
378 than-average air temperatures after the 8.2 ka event provided by a Central European  $\delta^{18}\text{O}$  record, *Quat. Sci. Rev.*, 172,  
379 96–108, <http://dx.doi.org/10.1016/j.quascirev.2017.08.001>, 2017.
- 380 Banner, J. L., Guilfoyle, A., James, E. W., Stern, L. A., and Musgrove, M.: Seasonal variations in modern speleothem  
381 calcite growth in central Texas, USA, *J. Sediment. Res.*, 77, 615–622, <https://doi.org/10.2110/jsr.2007.065>, 2007.
- 382 Barber, D. C., Dyke, A., Hillaire-Marcel, C., Jennings, A. E., Andrews, J. T., and Kerwin, M. W.: Forcing of the cold  
383 event of 8,200 years ago by catastrophic drainage of Laurentide lakes, *Nature*, 400, 344, <https://doi.org/10.1038/22504>,  
384 1999.
- 385 Baker, A., Asrat, A., Fairchild, I. J., Leng, M. J., Wynn, P. M., Bryant, C., Genty, D., and Umer, M.: Analysis of the  
386 climate signal contained within  $\delta^{18}\text{O}$  and growth rate parameters in two Ethiopian stalagmites, *Geochim. Cosmochim.*  
387 *Acta.*, 71, 2975–2988, <https://doi.org/10.1016/j.gca.2007.03.029>, 2007.
- 388 Buizert, C., Sigl, M., Severi, M., Markle, B. R., Wettstein, J. J., and McConnell, J. R.: Abrupt ice-age shifts in southern  
389 westerly winds and Antarctic climate forced from the north, *Nature*, 563, 681–685, [https://doi.org/10.1038/s41586-](https://doi.org/10.1038/s41586-018-0727-5)  
390 018-0727-5, 2018.
- 391 Burstyn, Y., Martrat, B., Lopez, J. F., Iriarte, E., Jacobson, M. J., Lone, M. A., and Deininger, M.: Speleothems from  
392 the Middle East: an example of water limited environments in the SISAL database, *Quaternary*, 2, 16,  
393 <https://doi.org/10.3390/quat2020016>, 2019.
- 394 Cheng, H., Edwards, R. L., Shen, C. C., Polyak, V. J., Asmerom, Y., and Woodhead, J.: Improvements in  $^{230}\text{Th}$  dating,  
395  $^{230}\text{Th}$  and  $^{234}\text{U}$  half-life values, and U-Th isotopic measurements by multi-collector inductively coupled plasma mass  
396 spectrometry, *Earth. Planet. Sci. Lett.*, 371–372, 82–91, <https://doi.org/10.1016/j.epsl.2013.04.006>, 2013.
- 397 Cheng, H., Fleitmann, D., Edwards, R. L., Wang, X., Cruz, F. W., and Auler, A. S.: Timing and structure of the 8.2  
398 kyr B.P. event inferred from  $\delta^{18}\text{O}$  records of stalagmites from China, Oman, and Brazil, *Geology*, 37, 1007–1010,  
399 <https://doi.org/10.1130/G30126A.1>, 2009.
- 400 Cheng, H., Li, H., Sha, L., Sinha, A., Shi, Z., Yin, Q., Lu, Z., Zhao, D., Cai, Y., Hu, Y., Hao, Q., Tian, J., Kathayat,  
401 G., Dong, X., Zhao, J., and Zhang, H.: Milankovitch theory and monsoon, *Innovation*, 3, 100338,  
402 <https://doi.org/10.1016/j.xinn.2022.100338>, 2022.
- 403 Cheng, H., Zhang, H., Spotl, C., Baker, J., Sinha, A., and Li, H.: Timing and structure of the Younger Dryas event  
404 and its underlying climate dynamics, *Proc. Natl. Acad. Sci. USA.*, 117, 23408–23417,  
405 <https://doi.org/10.1073/pnas.2007869117>, 2020.
- 406 Cheng, H., Zhang, H., Cai, Y., Shi, Z., Yi, L., Deng, C., and Perez-Mejías, C.: Orbital-scale Asian summer monsoon  
407 variations: Paradox and exploration, *Sci. China. Earth. Sci.*, 64, 529–544, [https://doi.org/10.1007/s11430-020-9720-](https://doi.org/10.1007/s11430-020-9720-y)  
408 y, 2021.
- 409 Chiang, J. C., Fung, I. Y., Wu, C. H., Cai, Y., Edman, J. P., Liu, Y., and Labrousse, C. A.: Role of seasonal transitions  
410 and westerly jets in East Asian paleoclimate. *Quat. Sci. Rev.*, 108, 111–129,  
411 <https://doi.org/10.1016/j.quascirev.2014.11.009>, 2015.



- 412 Cruz, F., Burns, S., Jercinovic, M., Karmann, I., Sharp, W., and Vuille, M.: Evidence of rainfall variations in Southern  
413 Brazil from trace element ratios (Mg/Ca and Sr/Ca) in a Late Pleistocene stalagmite, *Geochem. Cosmochim. Acta.*,  
414 71, 2250–2263, <https://doi.org/10.1016/j.gca.2007.02.005>, 2007.
- 415 Daley, T. J., Street-Perrott, F. A., Loader, N. J., Barber, K. E., Hughes, P. D., Fisher, E. H., and Marshall, J. D.:  
416 Terrestrial climate signal of the “8200 yr BP cold event” in the Labrador Sea region, *Geology*, 37, 831–834,  
417 <https://doi.org/10.1130/G30043A.1>, 2009.
- 418 Domínguez-Villar, D., Fairchild, I. J., Baker, A., Wang, X., Edwards, R. L., and Cheng, H.: Oxygen isotope  
419 precipitation anomaly in the North Atlantic region during the 8.2 ka event, *Geology*, 37, 1095–1098,  
420 <https://doi.org/10.1130/G30393A.1>, 2009.
- 421 Dong, J., Shen, C. C., Kong, X., Wu, C. C., Hu, H. M., Ren, H., and Wang, Y.: Rapid retreat of the East Asian summer  
422 monsoon in the middle Holocene and a millennial weak monsoon interval at 9 ka in northern China, *J. Asian. Earth.*  
423 *Sci.*, 151, 31–39, <https://doi.org/10.1016/j.jseas.2017.10.016>, 2018.
- 424 Dorale, J. A., and Liu, Z.: Limitations of Hendy test criteria in judging the paleoclimatic suitability of speleothems  
425 and the need for replication, *J. Caves. Karst. Stud.*, 71, 73–80, 2009.
- 426 Duan, P., Li, H., Sinha, A., Voarintsoa, N. R. G., Kathayat, G., Hu, P., and Cheng, H.: The timing and structure of the  
427 8.2 ka event revealed through high-resolution speleothem records from northwestern Madagascar, *Quat. Sci. Rev.*,  
428 268, 107104, <https://doi.org/10.1016/j.quascirev.2021.107104>, 2021.
- 429 Duan, P., Li, H., Ma, Z., Zhao, J., Dong, X., Sinha, A., and Cheng, H.: Interdecadal to centennial climate variability  
430 surrounding the 8.2 ka event in North China revealed through an annually resolved speleothem record from Beijing,  
431 *Geophys. Res. Lett.*, 50, e2022GL101182, <https://doi.org/10.1029/2022GL101182>, 2023.
- 432 Duan, W., Ma, Z., Tan, M., Cheng, H., Edwards, R. L., and Wen, X.: Timing and structure of early-Holocene climate  
433 anomalies inferred from north Chinese stalagmite records, *Holocene*, 31, 1777–1785,  
434 <https://doi.org/10.1177/09596836211033218>, 2021.
- 435 Duan, W., Ruan, J., Luo, W., Li, T., Tian, L., and Zeng, G.: The transfer of seasonal isotopic variability between  
436 precipitation and drip water at eight caves in the monsoon regions of China, *Geochim. Cosmochim. Acta.*, 183, 250–  
437 266, <http://dx.doi.org/10.1016/j.gca.2016.03.037>, 2016.
- 438 Duan, W., Tan, M., Ma, Z., and Cheng, H.: The palaeoenvironmental significance of  $\delta^{13}\text{C}$  of stalagmite BH-1 from  
439 Beijing, China during Younger Dryas intervals inferred from the grey level profile, *Boreas*, 43, 243–250,  
440 <https://doi.org/10.1111/bor.12034>, 2014.
- 441 Edwards, R. L., Chen, J. H., and Wasserburg, G. J.:  $^{238}\text{U}$ - $^{234}\text{U}$ - $^{230}\text{Th}$ - $^{232}\text{Th}$  systematics and the precise measurement  
442 of time over the past 500,000 years, *Earth Planet. Sci. Lett.*, 81, 175–192, [https://doi.org/10.1016/0012-821X\(87\)90154-3](https://doi.org/10.1016/0012-821X(87)90154-3), 1987.
- 444 Ellison, C. R., Chapman, M. R., and Hall, I. R.: Surface and deep ocean interactions during the cold climate event  
445 8200 years ago, *Science*, 312, 1929–1932, <https://doi.org/10.1126/science.1127213>, 2006.
- 446 Fairchild, I. J., Borsato, A., Tooth, A. F., Frisia, S., Hawkesworth, C. J., Huang, Y., and Spiro, B.: Controls on trace  
447 element (Sr-Mg) compositions of carbonate cave waters: implications for speleothem climatic records, *Chem. Geol.*,  
448 166, 255–269, [https://doi.org/10.1016/S0009-2541\(99\)00216-8](https://doi.org/10.1016/S0009-2541(99)00216-8), 2000.



- 449 Fairchild, I. J., Smith, C. L., Baker, A., Fuller, L., Spötl, C., Matthey, D., Chem. Geol., McDermott, F.: Modification  
450 and preservation of environmental signals in speleothems, *Earth. Sci. Rev.*, 75, 105–153,  
451 <https://doi.org/10.1016/j.earscirev.2005.08.003>, 2006.
- 452 Fairchild, I. J., Chem. Geol., Treble, P. C.: Trace elements in speleothems as recorders of environmental change, *Quat.*  
453 *Sci. Rev.*, 449–468, <https://doi.org/10.1016/j.quascirev.2008.11.007>, 2009.
- 454 Fleitmann, D., Burns, S. J., Mudelsee, M., Neff, U., Kramers, J., Mangini, A., and Matter, A.: Holocene forcing of the  
455 Indian monsoon recorded in a stalagmite from southern Oman, *Science*, 300, 1737–1739,  
456 <https://doi.org/10.1126/science.1083130>, 2003.
- 457 Fohlmeister, J.: A statistical approach to construct composite climate records of dated archives, *Quat. Geochronol.*,  
458 14, 48–56, <https://doi.org/10.1016/j.quageo.2012.06.007>, 2012.
- 459 Gauthier, M. S., Kelley, S. E., and Hodder, T. J.: Lake Agassiz drainage bracketed Holocene Hudson Bay ice saddle  
460 collapse, *Earth Planet. Sci. Lett.*, 544, 116372, <https://doi.org/10.1016/j.epsl.2020.116372>, 2020.
- 461 Godbout, P. M., Roy, M., and Veillette, J. J.: High-resolution varve sequences record one major late-glacial ice  
462 readvance and two drainage events in the eastern Lake Agassiz-Ojibway basin, *Quat. Sci. Rev.*, 223, 105942,  
463 <https://doi.org/10.1016/j.quascirev.2019.105942>, 2019.
- 464 Godbout, P. M., Roy, M., and Veillette, J. J.: A detailed lake-level reconstruction shows evidence for two abrupt lake  
465 drawdowns in the late-stage history of the eastern Lake Agassiz-Ojibway basin, *Quat. Sci. Rev.*, 238, 106327,  
466 <https://doi.org/10.1016/j.quascirev.2020.106327>, 2020.
- 467 Griffiths, M., Drysdale, R., Gagan, M., Frisia, S., Zhao, J., Ayliffe, L., Hantoro, W., Hellstrom, J., Fischer, M., and  
468 Feng, Y.: Evidence for Holocene changes in Australian–Indonesian monsoon rainfall from stalagmite trace element  
469 and stable isotope ratios, *Earth Planet. Sci. Lett.*, 292, 27–38, <https://doi.org/10.1016/j.epsl.2010.01.002>, 2010.
- 470 He, C., Liu, Z., Otto-Bliesner, B. L., Brady, E. C., Zhu, C., Tomas, R., and Bao, Y.: Hydroclimate footprint of pan-  
471 Asian monsoon water isotope during the last deglaciation, *Sci. Adv.*, 7, eabe2611,  
472 <https://doi.org/10.1126/sciadv.abe2611>, 2021.
- 473 Hersbach, H., Bell, B., Berrisford, P., Hirahara, S., Horányi, A., and Muñoz-Sabater, J.: The ERA5 global reanalysis,  
474 *Q. J. R. Meteorol. Soc.*, 146, 1999–2049, <https://doi.org/10.1002/qj.3803>, 2020.
- 475 Hijma, M. P., and Cohen, K. M.: Timing and magnitude of the sea-level jump prelude the 8200 yr event, *Geology*,  
476 38, 275–278, <https://doi.org/10.1130/G30439.1>, 2010.
- 477 Huguen, K. A., Overpeck, J. T., Peterson, L. C., and Trumbore, S.: Rapid climate changes in the tropical Atlantic  
478 region during the last deglaciation, *Nature*, 380, 51–54, <https://doi.org/10.1038/380051a0>, 1996.
- 479 Jansson, K. N., and Kleman, J.: Early Holocene glacial lake meltwater injections into the Labrador Sea and Ungava  
480 Bay, *Paleoceanography*, 19, PA1001, <https://doi.org/10.1029/2003PA000943>, 2004.
- 481 Jennings, A., Andrews, J., Pearce, C., Wilson, L., and Ólafsdóttir, S.: Detrital carbonate peaks on the Labrador shelf,  
482 a 13–7 ka template for freshwater forcing from the Hudson Strait outlet of the Laurentide Ice Sheet into the subpolar  
483 gyre, *Quat. Sci. Rev.*, 107, 62–80, <https://doi.org/10.1016/j.quascirev.2014.10.022>, 2015.



- 484 Johnson, K. R., Hu, C., Belshaw, N. S., and Henderson, G. M.: Seasonal trace-element and stable-isotope variations  
485 in a Chinese speleothem: The potential for high-resolution paleomonsoon reconstruction, *Earth Planet. Sci. Lett.*, 244,  
486 394–407, <https://doi.org/10.1016/j.epsl.2006.01.064>, 2006.
- 487 Kerwin, M. W.: A regional stratigraphic isochron (ca. 8000 <sup>14</sup>C yr BP) from final deglaciation of Hudson Strait, *Quat*  
488 *Res.*, 46, 89–98, <https://doi.org/10.1006/qres.1996.0049>, 1996.
- 489 Kleiven, H. K. F., Kissel, C., Laj, C., Ninnemann, U. S., Richter, T. O., and Cortijo, E.: Reduced North Atlantic deep  
490 water coeval with the glacial Lake Agassiz freshwater outburst, *Science*, 319, 60–64,  
491 <https://doi.org/10.1126/science.1148924>, 2008.
- 492 Kobashi, T., Menviel, L., Jeltsch-Thömmes, A., Vinther, B. M., Box, J. E., and Muscheler, R.: Volcanic influence on  
493 centennial to millennial Holocene Greenland temperature change, *Sci. Rep.*, 7, 1–10, <https://doi.org/10.1038/s41598-017-01451-7>, 2017.
- 495 Kobashi, T., Severinghaus, J. P., Brook, E. J., Barnola, J.-M., and Grachev, A. M.: Precise timing and characterization  
496 of abrupt climate change 8200 years ago from air trapped in polar ice, *Quat. Sci. Rev.*, 26, 1212–1222,  
497 <https://doi.org/10.1016/j.quascirev.2007.01.009>, 2007.
- 498 Krklec, K., and Dominguez-Villar, D.: Quantification of the impact of moisture source regions on the oxygen isotope  
499 composition of precipitation over Eagle Cave, central Spain, *Geochim. Cosmochim. Acta.*, 134, 39–54,  
500 <https://doi.org/10.1016/j.gca.2014.03.011>, 2014.
- 501 Lajeunesse, P., and St-Onge, G.: The subglacial origin of the Lake Agassiz-Ojibway final outburst flood, *Nat. Geosci.*,  
502 1, 184–188, <https://doi.org/10.1038/ngeo130>, 2008.
- 503 Lawrence, T., Long, A. J., Gehrels, W. R., Jackson, L. P., and Smith, D. E.: Relative sea-level data from southwest  
504 Scotland constrain meltwater-driven sea-level jumps prior to the 8.2 kyr BP event, *Quat. Sci. Rev.*, 151, 292–308,  
505 <https://doi.org/10.1016/j.quascirev.2016.06.013>, 2016.
- 506 LeGrande, A. N., and Schmidt, G. A.: Ensemble, water isotope-enabled, coupled general circulation modeling insights  
507 into the 8.2 ka event, *Paleoceanography*, 23, PA3207, <https://doi.org/10.1029/2008PA001610>, 2008.
- 508 Li, H., Cheng, H., and Wang, J.: Applications of laser induced breakdown spectroscopy to paleoclimate research:  
509 reconstructing speleothem trace element records, *Quat Sci.*, 38, 1549–1551 (in Chinese), 2018.
- 510 Li, H., Sinha, A., Anquetil André, A., Spötl, C., Vonhof, H. B., Meunier, A., and Cheng, H.: A multimillennial climatic  
511 context for the megafaunal extinctions in Madagascar and Mascarene Islands, *Sci. Adv.*, 6, eabb2459,  
512 <https://doi.org/10.1126/sciadv.abb2459>, 2020.
- 513 Li, X., Cheng, H., Tan, L., Ban, F., Sinha, A., and Duan, W.: The East Asian summer monsoon variability over the  
514 last 145 years inferred from the Shihua Cave record, North China, *Sci. Rep.*, 7, 7078, <https://doi.org/10.1038/s41598-017-07251-3>, 2017.
- 516 Li, Y., Rao, Z., Xu, Q., Zhang, S., Liu, X., Wang, Z., and Chen, F.: Inter-relationship and environmental significance  
517 of stalagmite  $\delta^{13}\text{C}$  and  $\delta^{18}\text{O}$  records from Zhenzhu Cave, north China, over the last 130 ka, *Earth Planet. Sci. Lett.*,  
518 536, 116149, <https://doi.org/10.1016/j.epsl.2020.116149>, 2020.



- 519 Liu, D., Wang, Y., Cheng, H., Edwards, R. L., and Kong, X.: Cyclic changes of Asian monsoon intensity during the  
520 early mid-Holocene from annually-laminated stalagmites, central China, *Quat. Sci. Rev.*, 121, 1–10,  
521 <https://doi.org/10.1016/j.quascirev.2015.05.003>, 2015.
- 522 Liu, Y., Henderson, G. M., Hu, C., Mason, A. J., Charnley, N., and Johnson, K. R.: Links between the East Asian  
523 monsoon and north Atlantic climate during the 8,200 year event, *Nat. Geosci.*, 6, 117–120,  
524 <https://doi.org/10.1038/ngeo1708>, 2013.
- 525 Liu, Z., Wen, X., Brady, E. C., Otto-Bliesner, B., Yu, G., Lu, H., and Yang, H.: Chinese cave records and the East  
526 Asia summer monsoon, *Quat. Sci. Rev.*, 83, 115–128, <https://doi.org/10.1016/j.quascirev.2013.10.021>, 2014.
- 527 Lochte, A. A., Repschläger, J., Kienast, M., Garbe-Schönberg, D., Andersen, N., and Hamann, C.: Labrador Sea  
528 freshening at 8.5 ka BP caused by Hudson Bay Ice Saddle collapse, *Nat. Commun.*, 10, 1–9,  
529 <https://doi.org/10.1038/s41467-019-08408-6>, 2019.
- 530 Ma, Z., Cheng, H., Tan, M., Edwards, R. L., Li, H., and You, C.: Timing and structure of the Younger Dryas event in  
531 northern China, *Quat. Sci. Rev.*, 41, 83–93, <https://doi.org/10.1016/j.quascirev.2012.03.006>, 2012.
- 532 Matero, I. S. O., Gregoire, L. J., Ivanovic, R. F., Tindall, J. C., and Haywood, A. M.: The 8.2 ka cooling event caused  
533 by Laurentide ice saddle collapse, *Earth Planet. Sci. Lett.*, 473, 205–214, <https://doi.org/10.1016/j.epsl.2017.06.011>,  
534 2017.
- 535 Matero, I. S., Gregoire, L. J., and Ivanovic, R. F.: Simulating the Early Holocene demise of the Laurentide Ice Sheet  
536 with BISICLES (public trunk revision 3298), *Geosci. Model. Dev.*, 13, 4555–4577, <https://doi.org/10.5194/gmd-13-4555-2020>, 2020.
- 538 McDermott, F.: Palaeo-climate reconstruction from stable isotope variations in speleothems: a review, *Quat. Sci. Rev.*,  
539 23, 901–918, <https://doi.org/10.1016/j.quascirev.2003.06.021>, 2004.
- 540 Mjell, T. L., Ninnemann, U. S., Eldevik, T., and Kleiven, H. K. F.: Holocene multidecadal-to millennial-scale  
541 variations in Iceland-Scotland overflow and their relationship to climate, *Paleoceanography*, 30, 558–569,  
542 <https://doi.org/10.1002/2014PA002737>, 2015.
- 543 Morrill, C., Anderson, D. M., Bauer, B. A., Buckner, R., Gille, E. P., Gross, W. S., Hartman, M., and Shah, A.: Proxy  
544 benchmarks for intercomparison of 8.2 ka simulations, *Clim. Past.*, 9, 423–432, <https://doi.org/10.5194/cp-9-423-2013>,  
545 2013.
- 546 Morrill, C., Ward, E. M., Wagner, A. J., Otto-Bliesner, B. L., and Rosenbloom, N.: Large sensitivity to freshwater  
547 forcing location in 8.2 ka simulations., *Paleoceanography*, 29, 930–945, <https://doi.org/10.1002/2014PA002669>, 2014.
- 548 Peros, M., Collins, S., G'Meiner, A. A., Reinhardt, E., and Pupo, F. M.: Multistage 8.2 kyr event revealed through  
549 high-resolution XRF core scanning of Cuban sinkhole sediments, *Geophys. Res. Lett.*, 44, 7374–7381,  
550 <https://doi.org/10.1002/2017GL074369>, 2017.
- 551 Polyak, V. J., Rasmussen, J. B., and Asmerom, Y.: Prolonged wet period in the southwestern United States through  
552 the Younger Dryas, *Geology*, 32, 5–8, <https://doi.org/10.1130/G19957.1>, 2004.
- 553 Ramsey, C. B.: Deposition models for chronological records, *Quat. Sci. Rev.*, 27, 42–60,  
554 <https://doi.org/10.1016/j.quascirev.2007.01.019>, 2008.

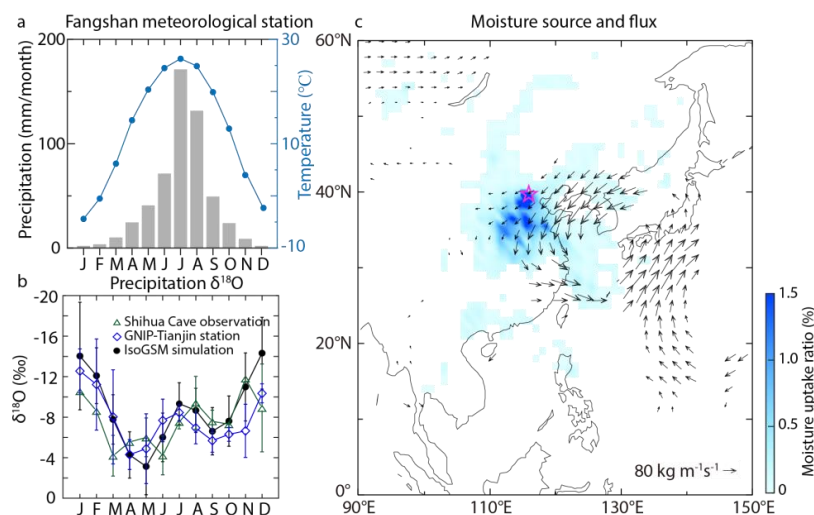




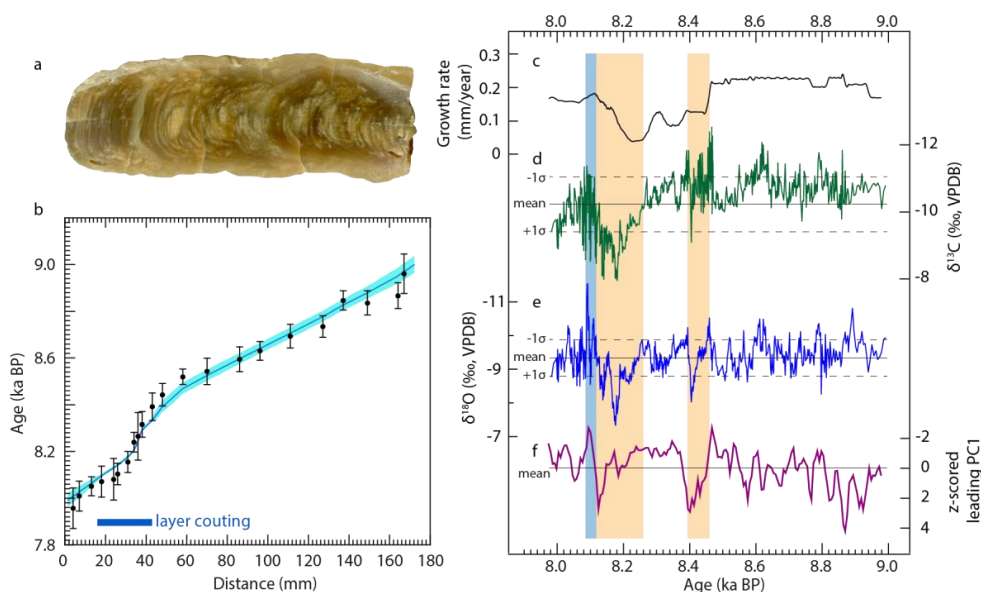
- 555 Renold, M., Raible, C. C., Yoshimori, M., and Stocker, T. F.: Simulated resumption of the North Atlantic meridional  
556 overturning circulation-slow basin-wide advection and abrupt local convection, *Quat. Sci. Rev.*, 29, 101–112,  
557 <https://doi.org/10.1016/j.quascirev.2009.11.005>, 2010.
- 558 Rohling, E. J., and Pälike, H.: Centennial-scale climate cooling with a sudden cold event around 8,200 years ago,  
559 *Nature*, 434, 975–979, <https://doi.org/10.1038/nature03421>, 2005.
- 560 Roy, M., Dell’Oste, F., Veillette, J. J., De Vernal, A., Hélié, J. F., and Parent, M.: Insights on the events surrounding  
561 the final drainage of Lake Ojibway based on James Bay stratigraphic sequences, *Quat. Sci. Rev.*, 30, 682–692,  
562 <https://doi.org/10.1016/j.quascirev.2010.12.008>, 2011.
- 563 Sodemann, H., Schwierz, C., and Wernli, H.: Interannual variability of Greenland winter precipitation sources:  
564 Lagrangian moisture diagnostic and North Atlantic Oscillation influence, *J. Geophys. Res. -Atmos.*, 113, D3107,  
565 <https://doi.org/10.1029/2007JD008503>, 2008.
- 566 Spurk, M., Leuschner, H. H., Baillie, M. G., Briffa, K. R., and Friedrich, M.: Depositional frequency of German  
567 subfossil oaks: climatically and non-climatically induced fluctuations in the Holocene, *Holocene*, 12, 707–715, 2002.
- 568 Stein, A. F., Draxler, R. R., Rolph, G. D., Stunder, B. J., Cohen, M. D., and Ngan, F.: NOAA’s HYSPLIT atmospheric  
569 transport and dispersion modeling system, *B. Am. Meteorol. Soc.*, 96, 2059–2077, [https://doi.org/10.1175/BAMS-D-](https://doi.org/10.1175/BAMS-D-14-00110.1)  
570 14-00110.1, 2015.
- 571 Steinhilber, F., Beer, J., Fröhlich, C.: Total solar irradiance during the Holocene, *Geophys. Res. Lett.*, 36,  
572 <https://doi.org/10.1029/2009GL040142>, 2009.
- 573 Stríkis, N. M., Cruz, F. W., Cheng, H., Karmann, I., Edwards, R. L., and Vuille, M.: Abrupt variations in South  
574 American monsoon rainfall during the Holocene based on a speleothem record from central-eastern Brazil, *Geology*,  
575 39, 1075–1078, <https://doi.org/10.1130/G32098.1>, 2011.
- 576 Tan, L., Li, Y., Wang, X., Cai, Y., Lin, F., Cheng, H., Ma, L., Sinha, A., and Edwards, R. L.: Holocene monsoon  
577 change and abrupt events on the western Chinese Loess Plateau as revealed by accurately dated stalagmites, *Geophys.*  
578 *Res. Lett.*, 47, e2020GL090273, <https://doi.org/10.1029/2020GL090273>, 2020.
- 579 Teller, J. T., Leverington, D. W., and Mann, J. D.: Freshwater outbursts to the oceans from glacial Lake Agassiz and  
580 their role in climate change during the last deglaciation, *Quat. Sci. Rev.*, 21, 879–887, [https://doi.org/10.1016/S0277-](https://doi.org/10.1016/S0277-3791(01)00145-7)  
581 3791(01)00145-7, 2002.
- 582 Thomas, E. R., Wolff, E. W., Mulvaney, R., Steffensen, J. P., Johnsen, S. J., and Arrowsmith, C.: The 8.2 ka event  
583 from Greenland ice cores, *Quat. Sci. Rev.*, 26, 70–81, <https://doi.org/10.1016/j.quascirev.2006.07.017>, 2007.
- 584 Törnqvist, T. E., and Hijma, M. P.: Links between early Holocene ice-sheet decay, sea-level rise and abrupt climate  
585 change, *Nat. Geosci.*, 5, 601–606, <https://doi.org/10.1038/ngeo1536>, 2012.
- 586 Voarintsoa, N. R. G., Matero, I. S., Railsback, L. B., Gregoire, L. J., Tindall, J., Sime, L., and Razanatsheho, M. O.  
587 M.: Investigating the 8.2 ka event in northwestern Madagascar: Insight from data-model comparisons, *Quat. Sci. Rev.*,  
588 204, 172–186, <https://doi.org/10.1016/j.quascirev.2018.11.030>, 2019.
- 589 Von Grafenstein, U., Erlernkeuser, H., and Trimborn, P.: Oxygen and carbon isotopes in modern fresh-water ostracod  
590 valves: assessing vital offsets and autecological effects of interest for palaeoclimate studies, *Palaeogeogr.*  
591 *Palaeoclimatol. Palaeoecol.*, 148, 133–152, [https://doi.org/10.1016/S0031-0182\(98\)00180-1](https://doi.org/10.1016/S0031-0182(98)00180-1), 1999.



- 592 Wagner, A. J., Morrill, C., Otto-Bliesner, B. L., Rosenbloom, N., and Watkins, K. R.: Model support for forcing of  
593 the 8.2 ka event by meltwater from the Hudson Bay ice dome, *Clim. Dyn.*, 41, 2855–2873,  
594 <https://doi.org/10.1007/s00382-013-1706-z>, 2013.
- 595 Wang, X., Auler, A. S., Edwards, R. L., Cheng, H., Cristalli, P. S., Smart, P. L., and Shen, C. C.: Wet periods in  
596 northeastern Brazil over the past 210 kyr linked to distant climate anomalies, *Nature*, 432, 740–743,  
597 <https://doi.org/10.1038/nature03067>, 2004.
- 598 Wanner, H., Solomina, O., Grosjean, M., Ritz, S. P., and Jetel, M.: Structure and origin of Holocene cold events, *Quat.*  
599 *Sci. Rev.*, 30, 3109–3123, <https://doi.org/10.1016/j.quascirev.2011.07.010>, 2011.
- 600 Wong, C. I., Banner, J. L., and Musgrove, M.: Holocene climate variability in Texas, USA: An integration of existing  
601 paleoclimate data and modeling with a new, high-resolution speleothem record, *Quat. Sci. Rev.*, 127, 155–173,  
602 <https://doi.org/10.1016/j.quascirev.2015.06.023>, 2015.
- 603 Yoshimura, K., Kanamitsu, M., Noone, D., and Oki, T.: Historical isotope simulation using reanalysis atmospheric  
604 data, *J. Geophys. Res. -Atmos.*, 113, D19108, <https://doi.org/10.1029/2008JD010074>, 2008.
- 605 Zhang, H., Griffiths, M. L., Chiang, J. C., Kong, W., Wu, S., Atwood, A., and Xie, S.: East Asian hydroclimate  
606 modulated by the position of the westerlies during Termination I, *Science*, 362, 580–583,  
607 <https://doi.org/10.1126/science.aat9393>, 2018.
- 608 Zhao, J., Cheng, H., Cao, J., Sinha, A., Dong, X., Pan, L., Pérez-Mejías, C., Zhang, H., Li, H., Wang, J., Wang, K.,  
609 Cui, J., and Yang, Y.: Orchestrated decline of Asian summer monsoon and Atlantic meridional overturning circulation  
610 in global warming period, *The Innovat. Geosci.*, 1, 100011, <https://doi.org/10.59717/j.xinn-geo.2023.100011>, 2023.



611  
612 **Figure 1. Climatology and locations.** (a) Climographs of precipitation amount (gray bars) and temperature (blue dots  
613 connected with lines) at Fangshan Station (39°46'N, 116°28'E) near the study site, based on Chinese Meteorological  
614 Administration data (<http://www.cma.gov.cn/>). (b) Annual cycle comparison of  $\delta^{18}\text{O}_p$  from observations of GNIP  
615 Tianjin station (<https://www.iaea.org/services/networks/gnip>) (1988–2002 with absent data covering 1993–2000, blue  
616 triangles), Shihua Cave (Duan et al., 2016) (2011–2014, green diamonds), and IsoGSM-simulation data (Yoshimura  
617 et al., 2008) (1979–2017, black dots) at the Huangyuan Cave. Error bars represent the  $1\sigma$  uncertainty of  $\delta^{18}\text{O}_p$  values  
618 for each month. (c) Mean July-August (JA) moisture source region (blue shading) the Hybrid Single Particle  
619 Lagrangian Integrated Trajectory (HYSPLIT) model version 4.0 (Stein et al., 2015) based on the NOAA-  
620 NCEP/NCAR reanalysis global meteorological field data of 2010–2020 (Sodemann et al., 2008; Krklec and  
621 Dominguez-Villar, 2014) and water vapor flux (arrow) from the European Centre for Medium-Range Weather  
622 Forecasts Reanalysis fifth-generation dataset (ERA5) (Hersbach et al., 2020) between 1980 and 2015.



623

624

625

626

627

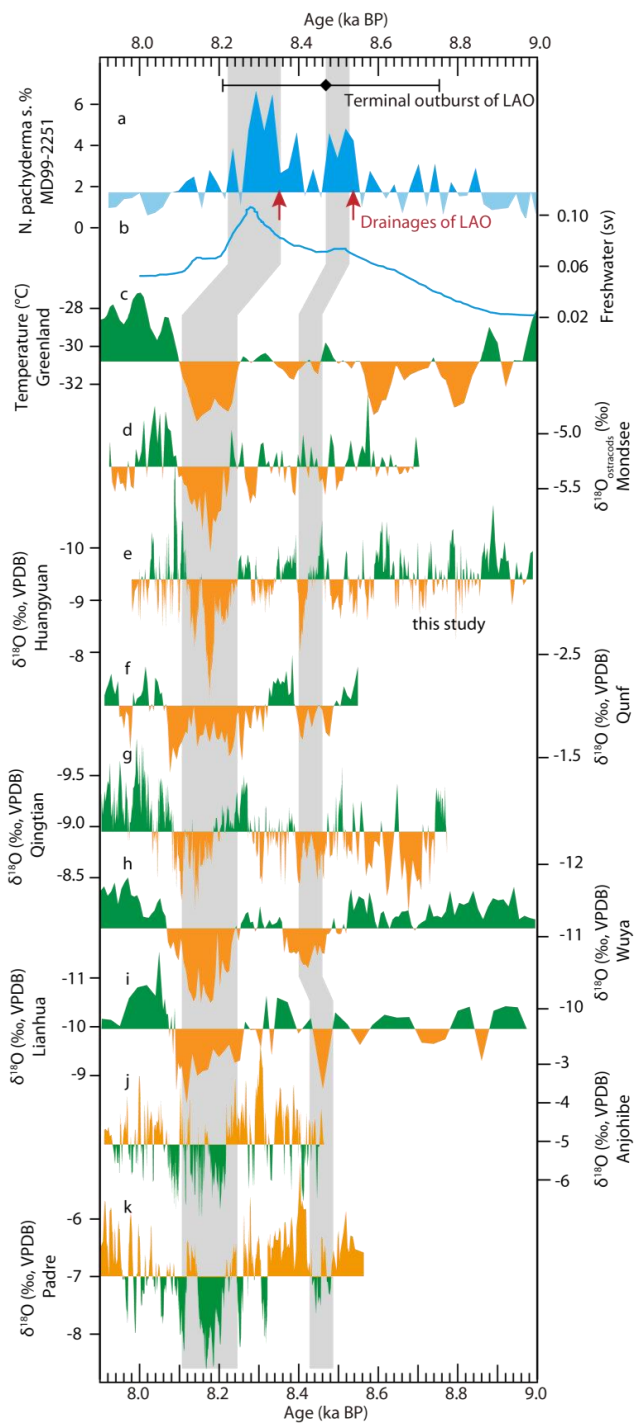
628

629

630

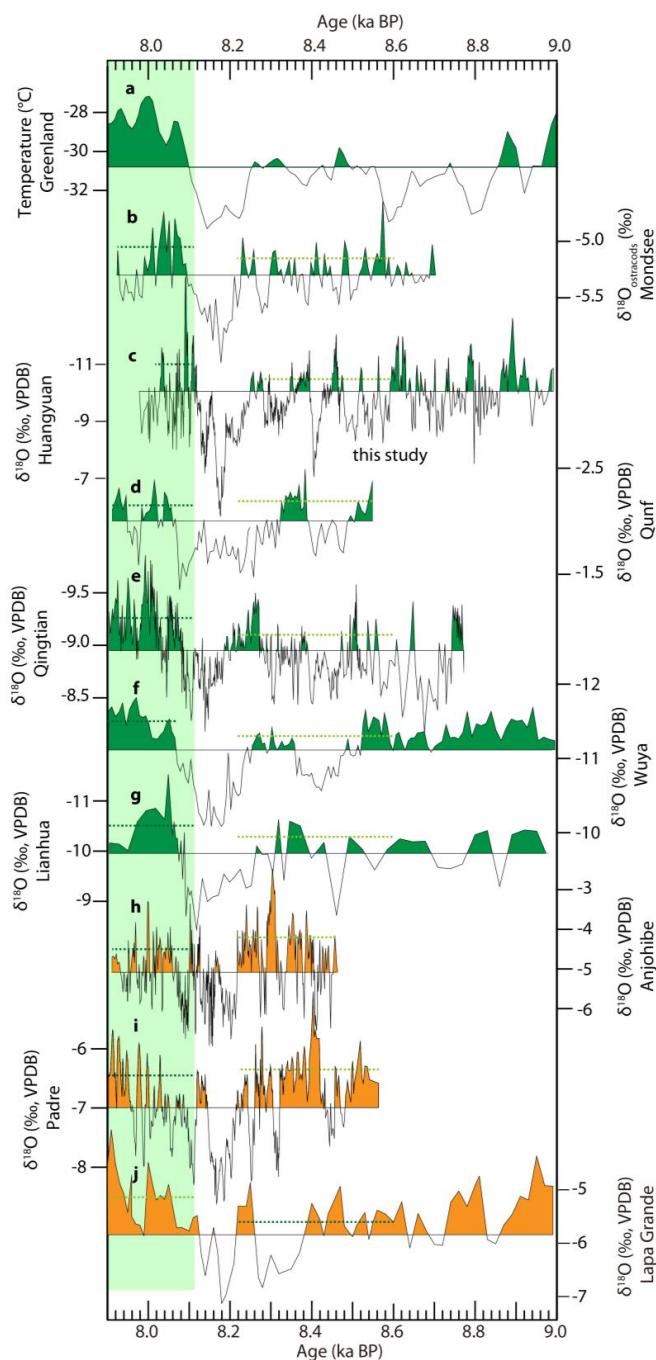
631

**Figure 2. Age model and proxy profiles of speleothem BH-2.** (a) Scanned image of speleothem BH-2. (b) Oxcal-derived age model (blue, Ramsey, 2008) with 95 % confidence interval (light blue shading). Black error bars on  $^{230}\text{Th}$  dates represent  $2\sigma$  analytical errors. The horizontal blue bar marks the range with layer counting. (c) The inferred growth rate of the BH-2 based on the chronology in (b). (d) and (e) are  $\delta^{18}\text{O}$  (dark blue) and  $\delta^{13}\text{C}$  (green) profiles, respectively. The mean (solid) and the  $\pm 1\sigma$  values (dashed) for each entire record are indicated by the horizontal lines. (f) 30-year loess filtered  $z$ -scored leading PC1 record of trace element ratios of Ba/Ca, Mg/Ca, and Sr/Ca (see Figure S2). The mean value of the PC1 record is presented. The vertical yellow bars in the right subpanel mark the anomalously positive episodes and the light blue bar indicates the subsequent  $\delta^{18}\text{O}$  overshoot after the 8.2 ka event.





633 **Figure 3. Comparisons of the BH-2  $\delta^{18}\text{O}$  record with records from circum-North Atlantic, ASM domain and**  
634 **South America. (a) *N.pachydermas.abundance* record from MD03-2665, North Atlantic (Ellison et al., 2006). The**  
635 **black diamond and error bar on the top indicate the dating of terminal outburst of LAO (Barber et al., 1999). The red**  
636 **arrows point to the two-step drainages of LAO into the North Atlantic. (b) Modelled freshwater flux from Laurentide**  
637 **Ice Sheet in unit of Sverdrups (Sv) (Matero et al., 2020). (c) Reconstructed temperature in Greenland (Kobashi et al.,**  
638 **2017). (d)  $\delta^{18}\text{O}_{\text{ostracods}}$  record from Modese, Austria (Andersen et al., 2017). (e) The BH-2  $\delta^{18}\text{O}$  record from**  
639 **Huangyuan Cave, Beijing (this study). (f) High-resolution  $\delta^{18}\text{O}$  record (Fleitmann et al., 2003) from Qunf Cave with**  
640 **more precise ages (Cheng et al., 2009) (g)  $\delta^{18}\text{O}$  record from Qingtian Cave, China (Liu et al., 2015). (h)  $\delta^{18}\text{O}$  record**  
641 **from Wuya Cave, Northwest China (Tan et al., 2020). (i)  $\delta^{18}\text{O}$  record from Lianhua Cave, North China (Dong et al.,**  
642 **2018). (j)  $\delta^{18}\text{O}$  record from Anjohibe Cave, Northwest Madagascar (Duan P et al., 2021). (k) High-resolution  $\delta^{18}\text{O}$**   
643 **record from Padre Cave, Brazil. The  $\delta^{18}\text{O}$  scale of j–k is inverse to other speleothem records. The vertical gray shading**  
644 **bars indicate the events centered at 8.4 and 8.2 ka BP.**  
645



646

647

648

649

**Figure 4. Comparisons of the overshoot between the BH-2  $\delta^{18}\text{O}$  record with other records. (a)** Reconstructed  
reconstructed temperature in Greenland (Kobashi et al., 2017). (b)  $\delta^{18}\text{O}_{\text{ostracods}}$  record from Modsee, Austria (Andersen et al.,  
2017). (c) The BH-2  $\delta^{18}\text{O}$  record from Huangyuan Cave, North China (this study). (d) High-resolution  $\delta^{18}\text{O}$  record



650 from Qunf Cave, Oman (Fleitmann et al., 2003; Cheng et al., 2009) based on more precise  $^{230}\text{Th}$  dates (Cheng et al.,  
651 2009). (e)  $\delta^{18}\text{O}$  record from Qingtian Cave, Central China (Liu et al., 2015). (f)  $\delta^{18}\text{O}$  record from Wuya Cave,  
652 Northwest China (Tan et al., 2020). (g)  $\delta^{18}\text{O}$  record from Lianhua Cave, North China (Dong et al., 2018). (h)  $\delta^{18}\text{O}$   
653 record from Anjohibe Cave, Northwest Madagascar (Duan P et al., 2021). (i) High-resolution  $\delta^{18}\text{O}$  record from  
654 Padre Cave, Brazil, on the Oxcal-derived chronology based on the  $^{230}\text{Th}$  dates of Cheng et al. (2009). (j)  $\delta^{18}\text{O}$  record  
655 from Lapa Grande Cave (Strikis et al., 2011) in Brazil. The  $\delta^{18}\text{O}$  scale of **h–j** is inverse to other speleothem records.  
656 The vertical green shading bar represents the overshoot episode following the 8.2 ka event. The  $\delta^{18}\text{O}$  value lower  
657 than the mean value of the entire records from the Northern Hemisphere, and Greenland reconstructed temperature  
658 record higher than the mean value of the entire record is shaded in green. The  $\delta^{18}\text{O}$  values higher than the mean  
659 value of the entire records from the Southern Hemisphere are shaded in brown. The green horizontal dashed lines in  
660 each record indicate the mean  $\delta^{18}\text{O}$  values for the age range they cover before (8.60–8.22 ka BP) and after (8.10–  
661 7.90 ka BP) the 8.2 ka event.